REFLECTION MOVEOUT INVERSION IN AZIMUTHALLY ANISOTROPIC MEDIA: ACCURACY, LIMITATION, AND ACQUISITION

AbdulFattah Al-Dajani

Earth Resources Laboratory
Department of Earth, Atmospheric, and Planetary Sciences
Massachusetts Institute of Technology
Cambridge, MA 02139

Tariq Alkhalifah

Stanford Exploration Project
Stanford University
Stanford, CA 93405

Dale Morgan

Earth Resources Laboratory
Department of Earth, Atmospheric, and Planetary Sciences
Massachusetts Institute of Technology
Cambridge, MA 02139

ABSTRACT

Parameter estimation from elliptical variations in the normal-moveout (NMO) velocity in azimuthally anisotropic media is sensitive to the angular separation between the survey lines in 2D, or equivalently source-to-receiver azimuth in 3D, and to the set of azimuths used in the inversion procedure. The accuracy in estimating the orientation of the NMO ellipse, the parameter α, in particular, is also sensitive to the strength of anisotropy.

To invert for the parameters the NMO ellipse, at least three NMO-velocity measurements along distinct azimuth directions are needed. In order to maximize the accuracy and stability in parameter estimation, it is best to have the azimuths for the three source-to-receiver directions 60° apart. Having more than three distinct source-

to-receiver azimuths (e.g., full azimuthal coverage) provides a useful data redundancy that enhances the quality of the estimates.

In orthorhombic media, inverting for the semi-axes of the NMO-ellipse allows the computation of the difference in the anisotropic parameters $\delta^{(1)}$ and $\delta^{(2)}$. Additional information such as well data, is necessary in order to determine $\delta^{(1)}$ and $\delta^{(2)}$. Furthermore, the accuracy in estimating the semi-axes of the NMO-velocity ellipse is about the same for any strength of anisotropy.

To maximize quality in the inversion process, it is recommended that at the design stage of seismic data acquisition to have small sector sizes ($\leq 10°$) with adequate fold and offset distribution.

For three azimuth directions, 60° apart, to perform the inversion, an azimuthally anisotropic layer overlain by an azimuthally isotropic overburden (as might happen for fractured reservoirs) should have a time thickness, relative to the total time, of at least the ratio of the error in the NMO (stacking) velocity to the interval anisotropy strength of the fractured layer. Coverage along more than three azimuths, however, improves this limitation, which is imposed by Dix differentiation, by at most 50% depending on the number of observations (NMO Velocities) that enter the inversion procedure.

INTRODUCTION

The model of transverse isotropy with horizontal symmetry-axis (HTI medium) is the simplest azimuthally anisotropic model used to describe vertically fractured reservoirs. The two orthogonal vertical symmetry planes that characterize the HTI model are: the symmetry-axis plane, which contains the symmetry-axis (perpendicular to the cracks) and the isotropy plane (parallel to the cracks).

Deviations from circular crack shape, misalignment of crack planes, the addition of a second crack system or the presence of anisotropy in the matrix make the azimuthal anisotropy more complicated (e.g., orthorhombic or lower order of symmetry). It is believed that one of the most common reasons for orthorhombic anisotropy in sedimentary basins is a combination of parallel vertical cracks and vertical transverse isotropy (VTI) in the background medium (Wild and Crampin, 1991). Orthorhombic symmetry can also be caused by two or three mutually orthogonal crack systems or two identical systems of cracks making an arbitrary angle with each other. Hence, orthorhombic anisotropy is expected to be closer to realistic fractured media. Analogous to Thomsen's (1986) notation for transverse isotropy with a vertical axis of symmetry (VTI), Tsvankin (1997) introduced a convenient notation to describe reflection moveout in orthorhombic media.

The presence of azimuthal anisotropy in practice has been documented in several studies such as those by Lynn *et al.* (1995) and Mallick *et al.* (1996). With the increased use of multicomponent seismic surveys and with close attention being paid to fractured-reservoir characterization in making hydrocarbon drilling and production decisions, azimuthal anisotropy has attracted the interest of researchers (e.g., Crampin *et*

al., 1980; Thomsen, 1988, 1995: Sena, 1991; Rüger, 1995; Tsvankin, 1995, 1997).

Tsvankin (1995) derived an analytic equation for the NMO velocity for a transversely isotropic medium with a horizontal axis of symmetry (HTI). Later, Al-Dajani and Tsvankin (1996) introduced an exact expression for the quartic coefficient of the Taylor's series expansion of the two-way traveltime for HTI media. Grechka and Tsvankin (1996) derived an analytic expression for the NMO velocity that is valid for pure mode propagation in an arbitrary azimuthally anisotropic layer with arbitrary strength of anisotropy. They showed that the azimuthal variation of the NMO velocity, in general, is elliptical. Recently, Al-Dajani *et al.* (1998) introduced a general analytic representation for long-spread (large offsets) reflection moveout for pure-mode of wave propagation in azimuthally anisotropic media. The analytic developments in Al-Dajani and Tsvankin (1996) and in Al-Dajani *et al.* (1998) have direct applications in performing a reflection moveout inversion for azimuthally anisotropic media.

The inversion for the parameters of azimuthally anisotropic media has been limited mostly to shear-wave splitting analysis with the goal of estimating the crack orientation and the crack density. One of the few parameter-estimation algorithms based on moveout analysis of P-wave data was presented by Sena (1991); however, Sena's method is limited to weak anisotropy and requires knowledge of the vertical velocity.

In their study, Al-Dajani and Alkhalifah (1997) discuss the inverse problem of using the azimuthal dependence of the NMO velocity in HTI media to invert for the HTI parameters. For P-wave propagation in HTI media, the medium parameters are: the fracture orientation α, the anisotropy parameter $\delta^{(V)}$, and the vertical velocity V_{Pvert}. Studying the estimation of HTI parameters, however, is very specific and it is not representative for the majority of azimuthal anisotropy cases.

Here, we generalize the study to more general anisotropic media by focusing on the parameters of the NMO-ellipse. The error analysis provides insight into the inverse problem and how it relates to seismic data acquisition. We explore the limitations involved in using the azimuthal variation in the NMO velocity to invert for the medium parameters. Moreover, we address issues such as the effect of sectorization in 3-D seismic data surveys on such inversion. Finally, we study how the resolution of the inverse problem is influenced by the number of NMO velocities that enter the inversion process. Our analysis concentrates on P–wave reflection moveout in azimuthally anisotropic media.

NORMAL MOVEOUT VELOCITY IN ANISOTROPIC MEDIA

The normal-moveout (NMO) velocity in azimuthally anisotropic media is elliptical, as shown by Grechka and Tsvankin (1996):

$$V^2_{\text{nmo}}(\alpha) = \frac{V^2_{\text{s1}} V^2_{\text{s2}}}{V^2_{\text{s1}} \sin^2\alpha + V^2_{\text{s2}} \cos^2\alpha}, \tag{1}$$

where V_{s1} and V_{s2} are the NMO velocities in the two vertical symmetry planes, and α is the angle between one of the symmetry planes and the survey line in 2D acquisition (or equivalently, source-to-receiver orientation in 3D acquisition). Clearly, from equation (1), V_{s1} and V_{s2} are the semi-axes of the NMO ellipse.

For pure P–wave propagation in HTI media, $V_{s1} = V_{Pvert}\sqrt{1+2\delta^{(V)}}$, $V_{s2} = V_{Pvert}$, and α in this case is the angle between the symmetry-axis plane and the survey line direction. Here, V_{Pvert} is the vertical P–wave velocity, while $\delta^{(V)}$ is Thomsen's parameter δ for the equivalent VTI medium along the symmetry-axis plane [see Tsvankin (1995) or Rüger (1995) for more information about the HTI notation]. For pure S–wave propagation, similar expressions exist (Tsvankin, 1995).

In orthorhombic media, the two semi-axes of the NMO ellipse are given by Grechka and Tsvankin (1996) for pure P–wave propagation as $V_{s1} = V_{P0}\sqrt{1+2\delta^{(1)}}$ and $V_{s2} = V_{P0}\sqrt{1+2\delta^{(2)}}$. Here, V_{P0} is the vertical P–wave velocity, $\delta^{(1)}$ and $\delta^{(2)}$ are dimensionless anisotropic parameters in the two symmetry planes defined in the same fashion as the δ parameter of Thomsen (1986) for VTI media [a complete description of this notation is given in Tsvankin (1997)]. α in this case is the angle between the survey line direction (or, source-to-receiver azimuth) and the symmetry plane associated with V_{s1}. Analogous expressions exist for S–wave propagation (see Tsvankin, 1997).

In 3-D (or, 2-D) land acquisition surveys or even water-bottom cable surveys, we have relatively full control on offset and azimuthal coverage. In conventional marine surveys, however, the azimuthal coverage is quite limited. It should be mentioned that constructing a common-mid-point (CMP) gather for a specific azimuthal direction in a 3-D acquisition survey requires, in general, collecting (sorting) traces from a range of azimuths (sectors). Since the azimuthal variation of the NMO velocity is elliptical, three NMO velocity estimates along three distinct source-to-receiver azimuths are necessary as well as sufficient to reconstruct the NMO ellipse and to invert for the parameters of the NMO ellipse: the NMO velocities along the two vertical symmetry planes (V_{s1}, V_{s2}), and the orientation of the NMO ellipse (α). Here, we investigate the choice of azimuth ranges for the optimum azimuthal directions that provide best inversion results. The maximum azimuthal separation between any two survey lines, in 2-D, or any two source-to-receiver azimuths, in 3-D, is 120°. Therefore, setting two of the three required azimuths 120° apart is an interesting choice to study. Moreover, conventional seismic data acquisitions utilize, in many cases, orthogonal directions (e.g., perpendicular strike and dip). Hence, a 90° azimuthal separation is another choice of interest. In many cases, however, the azimuthal coverage is small. Therefore, a choice of narrow azimuthal separation between the seismic lines is also addressed.

ERROR ANALYSIS

To estimate the sensitivity of the NMO velocity to the NMO ellipse parameters, we evaluate the Jacobian of equation (1). The Jacobian is obtained by calculating the derivatives of NMO velocity with respect to the ellipse parameters V_{s1}, V_{s2}, and α. Al-

though the NMO-velocity in equation (1) is nonlinear, its dependence on the anisotropy parameters is smooth enough to use the Jacobian for developing insight into the inverse problem. The derivatives used to form the Jacobian are as follows:

$$d_1(\alpha) = \frac{V_{s1}}{V_{nmo}(\alpha)} \frac{\partial V_{nmo}(\alpha)}{\partial V_{s1}},$$

$$d_2(\alpha) = \frac{V_{s2}}{V_{nmo}(\alpha)} \frac{\partial V_{nmo}(\alpha)}{\partial V_{s2}},$$

$$d_3(\alpha) = \frac{1}{V_{nmo}(\alpha)} \frac{\partial V_{nmo}(\alpha)}{\partial \alpha}.$$

The normalization of the derivatives chosen here simplifies the comparison of the contribution of each parameter to the NMO velocity. As a result, the information provided by these derivatives consists of relative values for V_{s1}, V_{s2} and absolute value for α (measured in radians). Therefore, the Jacobian matrix can be computed at three distinct azimuths (α_1, α_2, and α_3, measured relative to the minor semi-axis).

The sensitivity of the inversion to errors in the input data (NMO velocities) can be estimated using the Jacobian matrix

$$J = \begin{pmatrix} d_1(\alpha_1) & d_2(\alpha_1) & d_3(\alpha_1) \\ d_1(\alpha_2) & d_2(\alpha_2) & d_3(\alpha_2) \\ d_1(\alpha_3) & d_2(\alpha_3) & d_3(\alpha_3) \end{pmatrix},$$

where α_1, α_2, and α_3 are the azimuths of the CMP gathers relative to one of the two vertical symmetry planes (e.g., the plane that contains the minor semi-axis of the NMO ellipse).

The condition number for the Jacobian matrix provides an approximate overall estimate of the quality (stability) of the inversion for all three parameters. We will use the condition number as a criterion to design the best experimental setup. Error propagation (covariance) analysis, on the other hand, provides insight into both the accuracy and resolution of the inverse problem and how they relate to the error in the input NMO velocities and seismic data acquisition. Let us look at the expected performance of the inversion from both point of view.

Conditioning of the Problem

The reciprocal of the condition number, κ^{-1}, for the Jacobian matrix J is given by

$$\kappa^{-1} = \sqrt{\frac{|\lambda_{min}|}{|\lambda_{max}|}}, \tag{2}$$

where λ_{max} and λ_{min} are the maximum and minimum eigenvalues, respectively, of the matrix $A = J^T J$ (J^T is the transpose of J).

A small value of κ^{-1} ($\approx$0) implies an ill-conditioned (i.e., nearly singular) problem, while a large value of κ^{-1} usually implies a well-conditioned problem.

Figure 1 shows the reciprocal of the condition number, κ^{-1} [equation (2)], as a function of one of the azimuths (α_2), and one of the semi-axes of the NMO ellipse (V_{s1}). Here, the other two input azimuths are set to have maximum angular separation: $\alpha_1 = 0°$ and $\alpha_3 = 120°$, while the other semi-axis V_{s2} is set to 2.0 km/s. Notice from Figure 1 that the problem is clearly singular, with κ^{-1}=0, when the third-line direction α_2 coincides with either of the other two azimuths (only two azimuths are available). Note also that when there is no azimuthal variation in NMO velocity ($V_{s1} = V_{s2}$), as in isotropic media, we obviously cannot resolve the directions of the symmetry planes, and again κ^{-1}=0. As we should expect, the ellipticity of the NMO-velocity function increases (i.e., stronger anisotropy) with increasing variation in the NMO velocities along the semi-axes. As seen in Figure 1, the stability improves with an increase in anisotropy, and the maximum of κ^{-1} (most stability) corresponds to the third-line direction α_2 being midway in between.

Let us study the azimuthal variation of the computed reciprocal of the condition number κ^{-1} for a set of three-survey-line orientations (or source-to-receiver azimuths) with a fixed angular separation, $\Delta\alpha$, where $\Delta\alpha = \alpha_3 - \alpha_2 = \alpha_2 - \alpha_1$. The survey lines are simultaneously rotated so that the middle line (angle α_2) spans the azimuthal range from 0° to 180° measured from the symmetry-axis direction. This study allows us to understand how well-behaved (conditioned) is the inverse problem as a function of both azimuth and angular separation between the lines.

Figure 2 shows the results of this study for five different angular separations, $\Delta\alpha$, between the lines: (a) 7.5°, (b) 15°, (c) 30°, (d) 45°, and (e) 60°. κ^{-1} shows the least variation with azimuth for the maximum angular separation ($\Delta\alpha = 60°$) between the survey lines (curve e in Figure 2). It should be mentioned that we should choose a survey design that has a higher overall stability for the whole range of azimuths, since we usually do not know in advance the direction of the symmetry planes. The azimuthal variation in κ^{-1} for $\Delta\alpha \leq 45°$, make those angular separations less desirable compared to the 60°.

Overall, the condition-number analysis shows that the widest angular separation between the azimuths (i.e., $\Delta\alpha = 60°$), as intuition may suggest, provides a well-conditioned (well-behaved) inverse problem for any orientation of the three lines.

In the following, we quantify propagation of errors to the NMO ellipse parameters for a given error in the input measurements (NMO velocity) via a study of the covariance matrix.

Error Propagation (Covariance Matrix)

The propagation of errors from the input measurements (NMO velocities) to the NMO velocity ellipse parameters can be analyzed by calculating the covariance matrix of this inverse problem.

The covariance for the least-squares estimates of the model parameters (from the NMO ellipse) can be formulated as (Tarantola, 1987; Al-Dajani and Alkhalifah, 1997):

$$C_{\mathrm{m}} = c_{\mathrm{d}}[J^T J]^{-1}\,, \tag{3}$$

where c_{d} is a single measurement representing the variance of the input data (NMO velocities), and J is the Jacobian matrix. Here, we assume no uncertainties other than those associated with the input NMO-velocity data, and that these input data uncertainties are independent, identically normally distributed with a known covariance.

We use the square-root of the diagonal elements of C_{m} to estimate the expected error (standard deviation) for each parameter: the absolute error in α measured in radians, the percentage error in V_{s1}, and the percentage error in V_{s2}. If we set c_{d} to unity, the diagonal elements of $[J^T J]^{-1/2}$ simply measure the magnification factors of the error in each parameter for any given error in the input NMO-velocity measurements (given in percent). The magnification factors of the errors for the three parameters are denoted as M_{α} (measured in radians), $M_{V_{\mathrm{s1}}}$ (dimensionless), and $M_{V_{\mathrm{s2}}}$ (dimensionless).

Similar to the analysis of the previous section, let us study the square-root of the covariance matrix (error propagation) as a function of the central azimuth, α_2, for three angular separations between the survey lines: $\Delta\alpha = 30°$, $45°$, and $60°$. The central azimuth, α_2, spans the angular range from $0°$ to $180°$ measured relative to the minor semi-axis of the NMO ellipse (V_{s1}). The variance of the input data (NMO-velocities) c_{d} in equation (3), as described above, is set to unity. The resulting magnification factors for the errors in each parameter are shown in Figures 3 and 4.

As demonstrated in Figure 3a, the accuracy in estimating the parameter α improves by a factor of about 3 by using an angular separation of $60°$, as opposed to $30°$, for most ranges of azimuths. For α_2 near the symmetry-plane directions, the error in α estimates, however, is about the same for the three angular separations. Where the symmetry-plane direction is not known in advance (as is most often the case), however, the behavior of the $30°$ angular separation is inappropriate. This indicates that the parameter α is quite sensitive to the set of azimuths used in the inversion procedure when $\Delta\alpha$ is small. The same observation we may conclude for $\Delta\alpha = 45°$, but to a lesser extent. The accuracy in estimating α for an angular separation of $60°$ is highest and is highly consistent for all orientations α_2. Notice again that the error in α varies inversely with the strength of anisotropy (Figure 3a compared to Figure 3b).

Figures 3c, d, e, and f demonstrate that the best accuracy in V_{s1} and V_{s2} for all azimuths is obtained using an angular separation of $60°$. The accuracy in resolving the semi-axes of the NMO-velocity ellipse, however, is about the same for the three angular separations for α_2 around the associated symmetry plane direction. It is interesting to observe that the accuracy in estimating V_{s1} (the minor semi-axis) slightly improves as the anisotropy becomes stronger (compare Figure 3c with Figure 3d). On the other hand, the accuracy in estimating V_{s2} (the major semi-axis) slightly improves as the anisotropy becomes weaker (compare Figure 3e with Figure 3f). The dependence of the accuracy in estimating V_{s1} and V_{s2} on the strength of anisotropy, however, becomes more significant

as the angular separation between the azimuths becomes smaller. Notice that with a 60° angular separation between the azimuths the accuracy in estimating V_{s1} and V_{s2} is about the same for different strength of anisotropy and with no significant magnification of the error.

To compute the expected absolute error (standard deviation) in the estimated symmetry planes directions (ellipse orientation), α, for a particular angular separation between the survey lines, we

- Pick the magnification factor for a given set of azimuths from Figures 3a,b.
- Multiply this factor by the error (standard deviation) in the input NMO-velocity measurements to get the absolute error in α (in radians).

Similarly, to estimate the percentage error in V_{s1}, we have to apply the same procedure but using Figures 3c and d. For V_{s2}, Figures 3e and f should be used to find the percentage error in this parameter.

Note that in typical seismic data acquisitions (land or even ocean-bottom), the azimuthal data coverage is quite flexible and having wide azimuth separation is feasible. Unfortunately, this is not the case with marine acquisition. In the marine case the maximum azimuthal coverage is about 30°. This case is simulated in details in Figure 4. Note the huge magnification of errors in these narrow azimuthal separations. Therefore, in marine seismic data acquisition, in order to ensure that our estimated parameters contains minimum errors we should have multiple direction shooting (60° apart).

Overall, from Figures 3 and 4, the best angular separation that should be used is, again, 60°.

It should be mentioned that in the more general case, considered here (e.g., orthorhombic media), using three P–wave NMO-velocity measurements along three distinct survey directions (azimuths), we can unambiguously identify the orientation and the semi-axes of the NMO-velocity ellipse (the NMO velocities along the symmetry planes). Unlike the HTI inverse problem (see Al-Dajani and Alkhalifah, 1997), we neither have the capability to distinguish between the two symmetry planes, nor to obtain individually the anisotropic parameters. However, we can estimate the difference between the anisotropic parameters $\delta^{(1)}$ and $\delta^{(2)}$.

In 3-D seismic data acquisition, constructing a CMP gather for a specific azimuthal direction in the survey requires collecting (sorting) traces from a range of azimuths (i.e., sectors). The residual time differences between the seismic traces within a sector influence the resolution of the NMO-velocity estimation. In the following we quantify the influence of the sector size on the resolution of the NMO velocity estimates. For simplicity, we consider the case where we have a homogeneous single orthorhombic layer with a horizontal interface.

SECTOR SIZE INDUCED ERROR

We can quantify the resolution (standard deviation) in the estimated NMO velocity due to sectorization as follows:

$$\text{Error}_{V_{\text{nmo}}} = \frac{1}{\bar{V}} \sqrt{\frac{1}{\Delta\alpha_s} \int_{\alpha_1}^{\alpha_3} (V_{\text{nmo}}(\alpha) - \bar{V})^2 d\alpha}\,, \tag{4}$$

where $\bar{V}$ is the average NMO velocity over the sector:

$$\bar{V} = \frac{1}{\Delta\alpha_s} \int_{\alpha_1}^{\alpha_3} V_{\text{nmo}}(\alpha) d\alpha\,,$$

and the sector size $\Delta\alpha_s$ is defined as:

$$\Delta\alpha_s = \alpha_3 - \alpha_1\,.$$

α_1 and α_3 are the azimuthal boundaries for any given sector, as seen in Figure 5. $V_{\text{nmo}}(\alpha)$ is given by the NMO ellipse equation (1). Using equation (4) we can quantify the standard deviation (error) in the NMO velocity for any given sector.

Figure 6 shows the results of computing the standard deviation in percent as a function of azimuth (α_2) for five different sector sizes: 5° (dashed gray), 10° (solid gray), 15° (dotted black), 30° (dashed black), and 45° (solid black). The central azimuth of the sector α_2 is used as a reference azimuth. The azimuthal variation (anisotropy) of the NMO velocity for this single and horizontal orthorhombic layer is 20% in Figure 6a, and it is 10% in Figure 6b. As shown by Figure 6, the narrower the sector size the more accurate estimates are obtained (e.g., 5°), as we should expect. The larger the sector size, on the other hand, the less resolution (more error) is obtained for the NMO velocity estimate (e.g., 45°). Ideally, the preference is to have the receiver lines aligned along the azimuth directions. It should be mentioned that the standard deviation of the NMO velocity is linearly proportional to the strength of anisotropy (Figure 6a compared to Figure 6b). Actually, we can state that the maximum induced-error is given by the following:

$$\text{Maximum Error}_{V_{\text{nmo}}} \approx \frac{\Delta\alpha_s}{2} \frac{\text{Anis.\%}}{100}\,, \tag{5}$$

where Anis. is the strength of anisotropy given in percent, and $\Delta\alpha_s$ is given in degrees. For example, according to equation (5) the maximum error that a 30° sector introduces into the NMO velocity which has an azimuthal anisotropy of 20% is about 3%. This result agrees with Figure 6.

As a result, it is recommended to use small sector sizes (e.g., 10° or less). It should be mentioned, however, that it is important at the design stage of seismic data acquisition to ensure that small sector sizes ($\leq 10°$) have adequate fold and offset distribution.

THE INVERSE PROBLEM IN LAYERED MEDIA

So far we have considered the inverse problem for a single, homogeneous, azimuthally anisotropic layer. Generally, however, a fractured zone that may be characterized by the HTI or orthorhombic symmetry is overlain by an overburden that may be inhomogeneous and anisotropic. In this section the inverse problem is studied for a model with an azimuthally isotropic overburden (e.g., purely isotropic, VTI, or both) above an orthorhombic layer. Once the interval NMO velocities in the orthorhombic layer have been found by conventional Dix differentiation (layer-stripping) of the moveout velocity from the top and bottom of the layer, we can apply the single-layer inversion discussed above. An additional question to be addressed, however, is the influence of the relative thickness of the azimuthally anisotropic layer (compared with the total thickness) on the stability and accuracy of the parameter estimation.

To set up the inverse problem, we consider the model shown in Figure 7, where the NMO velocity for reflections from the bottom of the azimuthally anisotropic layer is given by the Dix equation:

$$V_{\mathrm{N}}^2 = V_{\mathrm{N}-1}^2(1-\rho) + V_{\mathrm{nmo}}^2\rho\,, \tag{6}$$

with $V_{\mathrm{N}-1}$ being the NMO velocity for a reflection from the top of the orthorhombic layer, V_{nmo} is the interval NMO velocity of the orthorhombic layer given by equation (1), and $\rho = \Delta t_{\mathrm{N}}/T_{\mathrm{N}}$, is the ratio of the two-way interval traveltime Δt_{N} in the orthorhombic layer to the two-way total traveltime T_{N} from the surface to the bottom of the orthorhombic layer.

From equation (6), the interval NMO velocity for the azimuthally anisotropic layer can be represented as

$$V_{\mathrm{nmo}}^2 = \frac{V_{\mathrm{N}}^2 - V_{\mathrm{N}-1}^2(1-\rho)}{\rho}\,. \tag{7}$$

Therefore, the interval NMO velocity in the orthorhombic layer that will be estimated in the inversion process is dependent on the relative thickness of the layer ρ. This fact, which is well known from isotropic interval velocity analysis, influences the accuracy of the parameter estimation of the NMO ellipse in the orthorhombic layer. In order to gain more insight into this inverse problem, we conduct the following error analysis.

Error Analysis

To study the sensitivity of the effective NMO velocity to the NMO ellipse parameters of the orthorhombic layer and the layer thickness, we need to evaluate the Jacobian of equation (6). The derivatives used to form the Jacobian are

$$d_1(\alpha) = \frac{V_{\mathrm{N}-1}}{V_{\mathrm{N}}(\alpha)}\frac{\partial V_{\mathrm{N}}(\alpha)}{\partial V_{\mathrm{N}-1}}\,,$$

$$d_2(\alpha) = \frac{V_{s1}}{V_N(\alpha)} \frac{\partial V_N(\alpha)}{\partial V_{s1}},$$

$$d_2(\alpha) = \frac{V_{s2}}{V_N(\alpha)} \frac{\partial V_N(\alpha)}{\partial V_{s2}},$$

and

$$d_4(\alpha) = \frac{1}{V_N(\alpha)} \frac{\partial V_N(\alpha)}{\partial \alpha}.$$

The normalization of the derivatives simplifies the assessment of the relative importance of each parameter. Hence, the information provided by these derivatives consists of relative values for V_{N-1}, V_{s1}, and V_{s2}, and the absolute values for α (measured in radians within the layer). Note that V_{N-1} is not an unknown (it is one of our measurements), but it is included in the Jacobian to simplify the analysis of the inverse problem.

The sensitivity of this inversion to errors in the input data (i.e., NMO velocity at the top and bottom of the azimuthally anisotropic layer) can be assessed from the Jacobian matrix

$$J = \begin{pmatrix} 1 & 0 & 0 & 0 \\ d_1(\alpha_1) & d_2(\alpha_1) & d_3(\alpha_1) & d_4(\alpha_1) \\ d_1(\alpha_2) & d_2(\alpha_2) & d_3(\alpha_2) & d_4(\alpha_2) \\ d_1(\alpha_3) & d_2(\alpha_3) & d_3(\alpha_3) & d_4(\alpha_3) \end{pmatrix},$$

where α_1, α_2, and α_3 are the azimuths of the CMP gathers measured from the minor semi-axis of the NMO ellipse of the Orthorhombic layer.

As shown above, to obtain maximum stability and accuracy, the best set of azimuths to use in the inversion process corresponds to the maximum angular separation, $\Delta\alpha = 60°$. This conclusion remains valid here as well. Hence, in the upcoming tests we set the azimuths to $\alpha_1 = 0°, \alpha_2 = 60°$, and $\alpha_3 = 120°$ to concentrate on the dependence of the inversion results on ρ and the strength of azimuthal anisotropy.

The stability of the inverse problem for this azimuthal separation, measured using the reciprocal of the condition number [equation (2)], is linearly proportional to the layer thickness ratio (ρ) for $\rho < 0.4$ (Figure 8). For $\rho > 0.4$, κ^{-1} flattens out, as seen in Figure 8. Also, as in the homogeneous case, the stability increases (approximately linearly) with an increase in the strength of anisotropy (compare Figure 8a with Figure 8b). As we expect, for small thickness ratios (e.g., $\rho < 0.1$) the inverse problem is ill-conditioned.

To study the propagation of error (standard deviation) into the NMO ellipse parameters of the azimuthally anisotropic layer as a function of the thickness ratio ρ for a given error in the input NMO-velocity measurements, we compute the covariance matrix [equation (3)] for the Jacobian matrix J of this inverse problem. The assumptions here are the same as those for the homogeneous case discussed earlier. Setting the variance of the input NMO-velocity measurements to unity means that the square-root of the covariance represents the magnification of error (standard deviation) in each parameter

for any given error (standard deviation) in the input NMO-velocity. Figure 9 shows the error magnification factors (the square-root of the diagonal elements of $[J^T J]^{-1/2}$) as a function of ρ: (a) magnification factor in the absolute error in α (M_α) measured in radians, (b) magnification factor in the percentage error in V_{s1} ($M_{V_{s1}}$), and (c) magnification factor in the percentage error in V_{s2} ($M_{V_{s2}}$). As seen in Figure 9, the magnification of error in each parameter is proportional to $1/\rho$. Thus, for $\rho < 0.4$ the resolution, measured by the square-root of the variance (i.e., standard deviation) in Figure 9, improves significantly (linearly) as ρ increases. For $\rho > 0.4$ the resolution remains almost the same, which is consistent with the results obtained from the reciprocal of the condition number.

Numerical Inversion in Layered Media

In this section we perform the nonlinear inversion of NMO velocity in layered media by means of the Newton-Raphson method and study the sensitivity of the results to errors in the input data as a function of ρ. The input data in this case are the NMO velocity at the top of the anisotropic layer and three NMO-velocity measurements along distinct azimuth directions at the bottom of the layer. Consider two models of an azimuthally anisotropic layer with different strengths of anisotropy: 10% and 20%; the NMO velocity at the top of the target layer $V_{N-1} = 2.0$ km/s. From the study of the single-layer model, azimuthal separation of 60° between the survey azimuths, in general, produces the best inversion results. Let us select here $\alpha_1 = 0°, \alpha_2 = 60°$, and $\alpha_3 = 120°$ to be the three source-to-receiver azimuths, measured relative to the minor semi-axis of the NMO ellipse (V_{s1}). From 100 trials with $\pm$ 3% range of random error introduced into the exact NMO velocities at the top and bottom of the azimuthally anisotropic layer, we obtain the perturbed interval NMO velocities (using Dix differentiation), which are then used to estimate the parameters of the NMO ellipse for the azimuthally anisotropic layer. The solutions (the mean and standard deviation) as a function of ρ are displayed in Figure 10. The results in a, c, and e of Figure 10 correspond to an azimuthally anisotropic layer with anisotropy strength of 20%, while those in b, d, and f correspond to a layer with anisotropy strength of 10%.

Consistent with the study of the covariance matrix, Figure 10 shows that the errors in the estimates do not change much for $\rho > 0.4$, and vary significantly (almost inversely) with ρ for small ρ. That is, for small thickness ratios ($\rho < 0.4$), the error in the parameter estimation is magnified by the factor $1/\rho$ compared to the error in the effective NMO velocity, as expected from equation (7).

The parameter α is better resolved for stronger anisotropy (Figures 10a and 10b) (e.g., the error bars for α become twice as large when the anisotropy strength changes from 20% to 10%). On the other hand, the improvement in the accuracy in estimating the semi-axes of the NMO ellipse (V_{s1} and V_{s2}) with stronger anisotropy is not as dramatic as that in α (Figures 10c, d, e, and f). As in the single-layer model, the absolute error measured by the error bars is almost the same for both values of anisotropy strength. Therefore, the relative error is smaller for stronger anisotropy.

As demonstrated by Figure 10, an azimuthally anisotropic layer overlain by an azimuthally isotropic overburden should have a relative thickness (in time) to the total thickness of at least equal to the ratio of the error in the NMO (stacking) velocity to the interval anisotropy strength. This allows the error bars to be small enough to see the azimuthal variation in the NMO velocity inside the azimuthally anisotropic layer. For example, for typical errors in the estimated NMO (stacking) velocity ($\leq 2\%$), as is the case in this numerical study, the minimum ratio of thickness (in time) of the azimuthally anisotropic layer to the total thickness, ρ, needed to resolve the three parameters with acceptable accuracy is at least about 0.2, when the anisotropy strength is 10%, and it is 0.1 when the anisotropy strength is 20% (Figure 10). It is important to mention, however, that parameter estimation may become unstable for layers with weak azimuthal anisotropy ($< 10\%$), especially for small values of ρ (≤ 0.1). The significant deviation of the mean from the true solution in Figures 10c–f for $\rho \leq 0.1$ could be interpreted as a direct indication of instability in the inversion process. Note that larger errors in the NMO-velocity estimates ($> 2\%$) cause the required minimum relative thickness of the azimuthally anisotropic layer, before obtaining acceptable inversion results, to be larger as well.

Therefore, to ensure that the error bars associated with the ellipse parameters are less than the true values in azimuthally anisotropic media, a minimum relative thickness (in time) required before we lose our confidence in this inversion method is controlled mainly by the limitation of layer stripping (Dix differentiation). Having three NMO velocity measurements, 60° apart, the relative thickness should be at least equal to the ratio of the error in the NMO (stacking) velocity over the strength of azimuthal anisotropy of the fractured layer.

So far, we have concentrated our analyses to study the accuracy and limitations when we have minimum number of input NMO (stacking) velocities (i.e., three) which are required to invert for the ellipse parameters. Coverage along other directions, however, adds some redundancy which is useful in enhancing the quality of the inversion process. In the following section we discuss the influence of having more than three NMO velocities on the accuracy and limitations of such inversion procedure.

MORE THAN THREE AZIMUTHS (NMO VELOCITIES)

In theory, with N number of observations (NMO velocities), the error bars (standard deviation) reduce by a factor of $1/\sqrt{N-1}$. In order to substantiate this statement let us assume, for simplicity, that the NMO ellipse coincides with the Cartesian coordinate system (i.e., the semi-axes of the NMO ellipse are parallel to the Cartesian's x_1 and x_2 axes). Furthermore, let us focus our attention to invert for the two parameters that define the ellipticity of the NMO ellipse (i.e., the semi-axes of the NMO ellipse: V_{s1} and V_{s2}). If the error bars associated with the two semi-axes of the NMO ellipse are equal or greater than the azimuthal variation of the NMO ellipse, then the true NMO ellipse cannot be distinguished. Here, we use the least square solution to best fit the

data points (NMO velocities) to an ellipse.

Consider for the moment an azimuthally anisotropic layer which has a 20% NMO-velocity variation between the two semi-axes ($V_{s1} = 2.4$ km/s, and $V_{s2} = 3.0$ km/s). For each of the N velocities that enters the inversion process, a $\pm$ 3 % range of random error is introduced into the exact NMO velocity [equation (1)]. Then, we obtain the best fit ellipse solution in a least square sense. We repeat the experiment 100 times to obtain a statistical measurement for the standard deviation (error bar) for each parameter. It should be mentioned that the standard deviation for the introduced errors in the input NMO velocity is about 1.7%. We conduct the experiment for different number of input NMO velocities (N). To obtain maximum accuracy and stability, as we have seen earlier, we choose that the N observations to be equally apart and that they span the whole azimuth range (i.e., 360°). For example, when $N = 36$, the NMO velocities are 10° apart. The results of this inversion for both semi-axes are displayed in Figure 11.

The black dots in Figure 11 are the computed error bars (standard deviation), in percent, for both semi-axes of the NMO ellipse [V_{s1} (a), and V_{s2} (b)] as a function of number of observations. The solid curve, on the other hand, is the expected (theoretical) behavior with $1/\sqrt{(N-1)}$ reduction factor. Not surprisingly, for this homogeneous case, the reduction in the error is indeed proportional to $1/\sqrt{(N-1)}$.

Consider a more realistic case where we have an azimuthally anisotropic layer overlain by an azimuthally isotropic overburden (Figure 7). Let us repeat the experiment we have conducted earlier in Figure 10. In this case, however, we fix the relative thickness to 0.1 and we invert for V_{s1} and V_{s2} of the target layer with different numbers of input NMO velocities. The strength of azimuthal anisotropy is 20%. The result of this study is displayed in Figure 12. Similar to Figure 11, the black dots in Figure 12 are the error bars, in percent, for the estimated V_{s1} (a), and V_{s2} (b) as a function of the number of input NMO velocities. Again, the input NMO velocities are selected to be equally apart. The solid curve is the expected behavior with $1/\sqrt{(N-1)}$ reduction factor. Interestingly, the reduction in the error is not proportional to $1/\sqrt{(N-1)}$. The error, however, reduces to a threshold value which is at most about 50% of the error which is obtained with minimum number of observations ($N = 3$). Notice that at relatively large number of observations (e.g., N $\geq$ 24), the reduction in the error is not significant. Therefore, to approach the maximum possible resolution in real applications, where the number of azimuths that can be obtained from 3-D seismic surveys is finite, we only need to have an adequate number of azimuths (e.g., N $\geq$ 24).

Overall, having NMO-velocity measurements greater than the minimum requirement (i.e., three) reduces the limitation imposed by Dix differentiation by at most 50%, depending on the available number of observations (N). For example, in the previous section we have stated that with three input NMO velocities, 60° apart, a 20% azimuthally anisotropic layer should have a relative thickness, in time, of at least 0.1 to obtain acceptable inversion results, provided that the error in the input NMO (stacking) velocities is about 2%. Having larger number of input NMO velocities (e.g., 36), at distinct azimuth orientations, reduces the required minimum relative thickness to about

0.05. Similarly, in the case of 10% azimuthally anisotropic layer and with adequate number of NMO-velocity measurements (e.g, 36), the required relative thickness can be reduced from 0.2, as seen in the previous section, to 0.1. Again, the error in the input NMO velocities is assumed to be about 2%. It should be mentioned, however, that the inversion process still might suffer from some instability for layers with small relative thickness values (e.g., $\rho < 0.05$), especially for relatively weak azimuthal anisotropy (e.g., $< 10\%$).

CONCLUSIONS

We have discussed reflection moveout inversion for azimuthally anisotropic media, with emphasis on P-wave reflection moveout. We have applied a condition number analysis as well as error analysis techniques to study the inverse problem.

Parameter estimation from variations in the moveout velocity in azimuthally anisotropic media is quite sensitive to the angular separation between the survey lines and also to the set of azimuths used in the inversion procedure. The accuracy in estimating the orientation of the symmetry planes, α, in particular, is sensitive to the strength of anisotropy, with error inversely proportional to the strength of anisotropy. The accuracy in estimating the semi-axes of the NMO-velocity ellipse is about the same for any strength of anisotropy.

NMO-velocity measurements obtained for three distinct survey azimuths are sufficient to invert for the three ellipse parameters (V_{s1}, V_{s2}, and α). In order to maximize the accuracy and stability in parameter estimation, it is best to have the azimuths for the three source-to-receiver directions 60° apart. The accuracy in resolving the parameters for an angular separation of 60° is consistent at all azimuths, and for most ranges of azimuths the associated errors are the least. Coverage along more than three directions, however, add redundancy which is useful in enhancing the quality of the inversion process.

In orthorhombic media, inverting for the semi-axes of the NMO-ellipse allows the computation of the difference in the anisotropic parameters $\delta^{(1)}$ and $\delta^{(2)}$. Additional information such as well data is necessary in order to determine $\delta^{(1)}$ and $\delta^{(2)}$.

Constructing a CMP gather for a specific azimuthal direction in a 3-D acquisition survey, however, requires collecting (sorting) traces from a range of azimuths (sectors). To maximize quality in the inversion process, it is recommended that at the design stage of seismic data acquisition to have small sector sizes ($\leq 10°$) with adequate fold and offset distribution. Ideally, the preference is to have the receiver lines aligned along the azimuth directions.

In 3-D land and ocean-bottom-cable acquisition, where the acquisition is relatively flexible, it is recommended to have azimuthal coverage along at least three directions, 60° apart. In conventional marine (streamer) surveys, on the other hand, the azimuthal coverage is quite limited. Therefore, in order to obtain the required coverage along the optimal azimuth directions (60° apart), multiple surveys are needed. Other acquisition

issues such as the bin size, line spacing, receiver interval, fold, etc, are the same as those in any typical seismic survey (see Stone, 1994). Moreover, issues such as the presence of coherent noise, signal-to-noise (S/N) ratio, lateral velocity heterogeneity, and structure also influence the estimation of NMO velocities from reflection moveout and the inversion for medium parameters.

Using three NMO-velocity measurements along three distinct azimuths, 60° apart, an azimuthally anisotropic layer overlain by an azimuthally isotropic overburden (as might happen for fractured reservoirs) should have a relative thickness (in time) to the total thickness of at least equal to the ratio of the error in the NMO (stacking) velocity to the interval anisotropy strength of the fractured layer. For example, a relative thickness (in time) with respect to the total thickness of at least 0.2 is needed in order to obtain acceptable estimates of the medium parameters, provided that the azimuthal variation in the interval NMO velocity within the azimuthally anisotropic layer is about 10% and the error in the input NMO velocity measurement is 2%. It should be mentioned, however, that a choice of small angular separation between the three azimuth directions (e.g., $\leq 30°$) makes the required relative thickness to become larger.

Coverage along more than three azimuths reduces the limitation imposed by Dix differentiation by at most 50%, depending on the available number of observations (NMO Velocities) that enter the inversion procedure. To approach the maximum possible resolution in real applications, where the number of azimuths that can be obtained from 3-D seismic surveys is finite, we only need to have an adequate number of azimuths (e.g., ≥ 24).

The conclusions made here for P–wave reflection moveout inversion are also valid for pure S–wave propagation. Finally, understanding the limitations involved in such inversion process emphasizes the importance of integrating other seismic exploration techniques, such as azimuthal amplitude-variation-with-offset analysis and borehole information, to reduce the ambiguity in the estimation of the medium parameters.

ACKNOWLEDGMENTS

We are grateful to Nafi Toksöz, John Olson, and Rama Rao from the Earth Resources Laboratory (ERL) at the Massachusetts Institute of Technology (MIT), and Ken Larner from the Colorado School of Mines for the useful discussions. We thank ERL, the Stanford Exploration Project (SEP) at Stanford University, and our sponsors for the motivated input and great support. Al-Dajani would like to acknowledge the financial support from the Saudi Arabian Oil Company (Saudi Aramco). Al-Dajani is grateful to Mahmoud Abdul Baqi and Hany Abu Khadra from Saudi Aramco for their invaluable support.

REFERENCES

Al-Dajani, A. and Alkhalifah, T., 1997. Reflection moveout inversion for azimuthally anisotropic media, *67th Ann. Internat. Mtg., Soc. Expl. Geophys., Expanded Abstracts* 1230–1233.

Al-Dajani, A. and Tsvankin, I., 1996. Nonhyperbolic reflection moveout for horizontal transverse isotropy, *66th Ann. Internat. Mtg., Soc. Expl. Geophys., Expanded Abstracts,* 1495–1498.

Al-Dajani, A., Tsvankin, I., and Nafi Toksöz, 1998. Nonhyperbolic reflection moveout for azimuthally anisotropic media, *68th Ann. Internat. Mtg., Soc. Expl. Geophys., Expanded Abstracts,* 1497–1482.

Crampin, S., McGonigle, R., and Bamford, D., 1980. Estimating crack parameters from observations of P-wave velocity anisotropy, *Geophysics, 45*, 345–360.

Grechka, A. and Tsvankin, I., 1996. 3-D description of normal moveout in anisotropic media, *66th Ann. Internat. Mtg., Soc. Expl. Geophys., Expanded Abstracts,* 1487–1490.

Lynn, H.B., Bates, C.R., Simon, K.M., Van Doc, R., 1995. The effects of azimuthal anisotropy in P-wave 3-D seismic, *65th Ann. Internat. Mtg., Soc. Expl. Geophys., Expanded Abstracts,* 727–730.

Mallick, S., Craft, K.L., Meister, L.J., and Chambers, R.E., 1996. Determination of the principal directions of azimuthal anisotropy from P-wave seismic data, *58th EAGE Expanded Abstracts.*

Rüger, A., 1995. P-wave reflection coefficients for transversely isotropic media with vertical and horizontal axis of symmetry, *65th Ann. Internat. Mtg., Soc. Expl. Geophys., Expanded Abstracts,* 278–281.

Sena, A.G., 1991. Seismic traveltime equations for azimuthally anisotropic and isotropic media: Estimation of internal elastic properties, *Geophysics, 56*, 2090–2101.

Stone, D.G., 1994. *Designing Seismic Surveys in Two and Three Dimensions,* Society of Exploration Geophysics, Tulsa.

Tarantola, A., 1987. *Inverse Problem Theory,* Elsevier Pub., New York.

Thomsen, L., 1986. Weak elastic anisotropy, *Geophysics, 51*, 1954–1966.

Thomsen, L., 1988. Reflection seismology over azimuthally anisotropic media, *Geophysics, 53*, 304–313.

Thomsen, L., 1995. Elastic anisotropy due to aligned cracks in porous rock, *Geophysical Prospecting, 43*, 805–830.

Tsvankin, I., 1995. Inversion of moveout velocities for horizontal transverse isotropy, *65th Ann. Internat. Mtg., Soc. Expl. Geophys., Expanded Abstracts,* 735–738.

Tsvankin, I., 1997. Anisotropic parameters and P-wave velocity for orthorhombic media, *Geophysics, 62*, 1292–1309.

Wild, P., and Crampin, S., 1991. The range of effects of azimuthal isotropy and EDA anisotropy in sedimentary basins, *Geophys. J. Intl., 107*, 513–529.

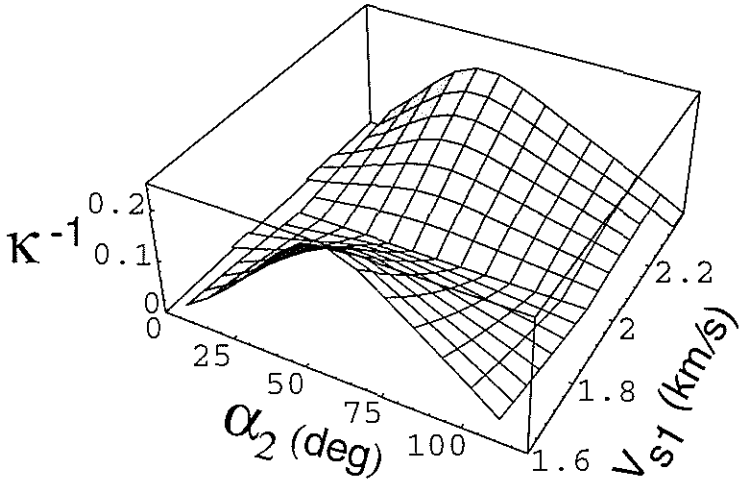

Figure 1: The reciprocal of the condition number (κ^{-1}) as a function of α_2 and V_{s1}. Here, α_1=0°, α_3=120°, and V_{s2} = 2.0 km/s.

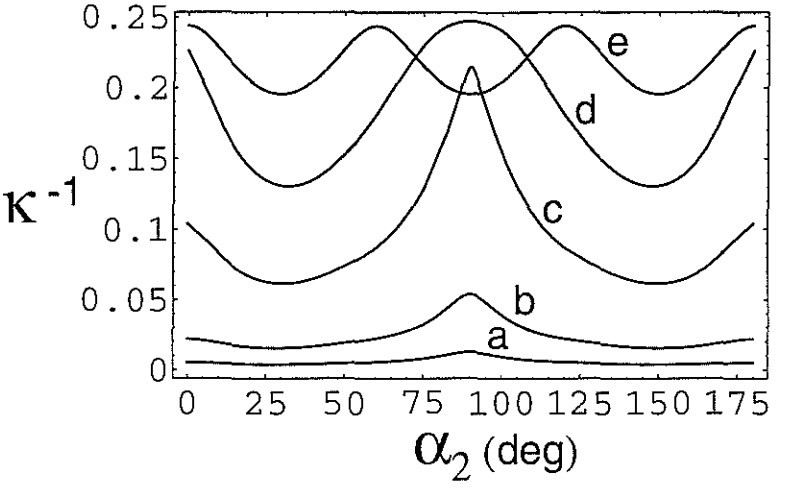

Figure 2: Reciprocal of the condition number (κ^{-1}) as a function of azimuth, α_2, for five different angular separations between three survey lines. Each set of azimuths is rotated so that the central line, α_2, spans the azimuths from 0° to 180° measured relative to the symmetry plane which is associated with the minimum NMO velocity (minor semi-axis of the NMO-velocity ellipse). The five curves correspond to $\Delta\alpha = 7.5°$ (a), 15° (b), 30° (c), 45° (d), and 60° (e). $V_{s1} = 1.6$ km/s, while $V_{s2} = 2.0$ km/s (corresponding to 20% NMO-velocity variation).

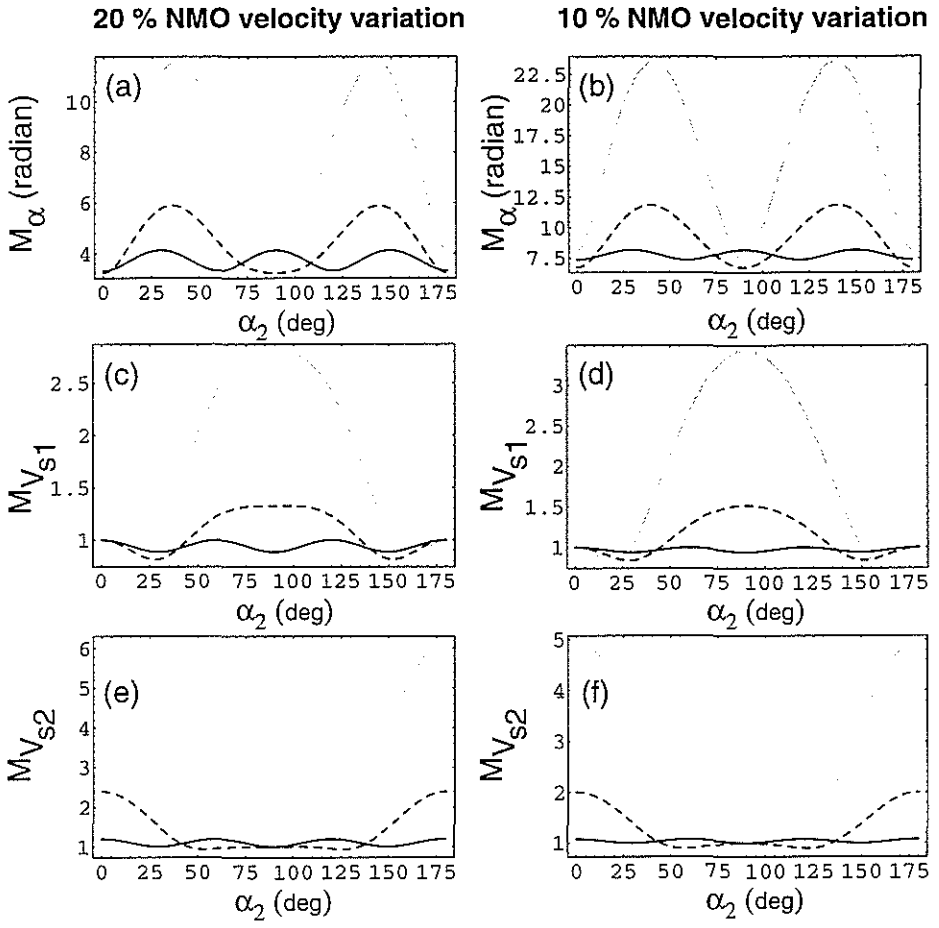

Figure 3: Magnification factor in the absolute error in α measured in radians, the percentage error in V_{s1}, and the percentage error in V_{s2} as functions of central azimuth α_2 for three different angular separations $\Delta\alpha$ between survey direction. The three sets of azimuth combinations are rotated so that the central azimuth spans azimuths from 0° to 180° measured from the symmetry-axis direction. The three curves correspond to angular separations of 30° (gray), 45° (dashed black), and 60° (solid black). The plots on the left column correspond to 20% NMO-velocity variation between the two vertical symmetry planes, while the plots on the right correspond to 10% NMO-velocity variation.

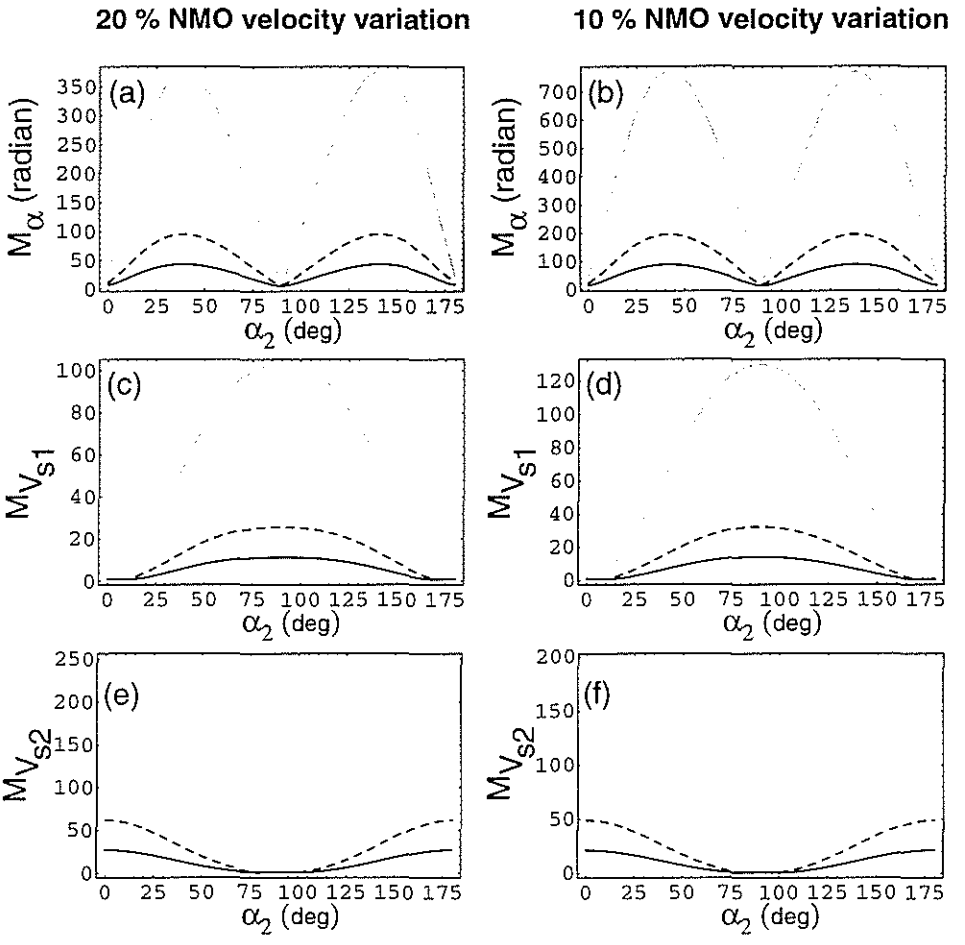

Figure 4: The same as Figure 3, but here the three curves correspond to angular separations of 5° (gray), 10° (dashed black), and 15° (solid black). The plots on the left column correspond to 20% NMO-velocity variation between the two vertical symmetry planes, while the plots on the right correspond to 10% NMO-velocity variation.

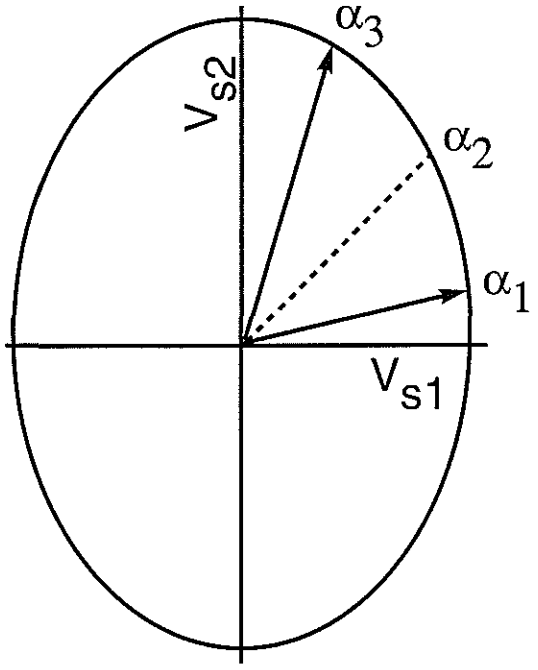

Figure 5: Schematic diagram showing a sector geometry imposed on the NMO-ellipse. α_1 and α_3 are the boundaries for the sector while α_2 is the central azimuth direction of the sector.

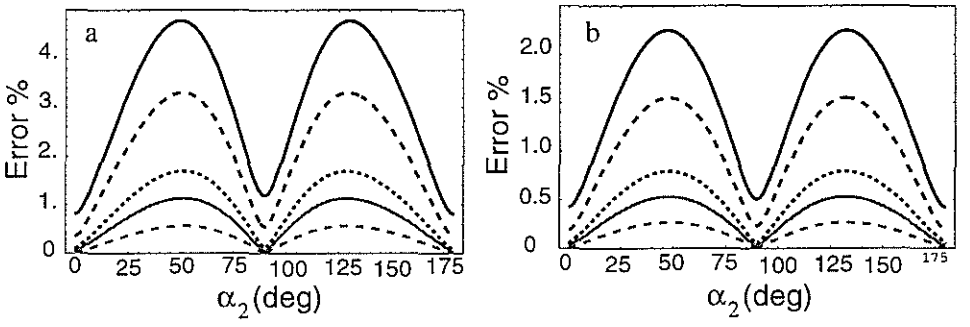

Figure 6: Azimuthal variation of the induced-error (standard deviation), given in percent, in the NMO velocity for five sector sizes: 5° (dashed gray), 10° (solid gray), 15° (dotted black), 30°(dashed black), and 45° (solid black); α_2 is the central azimuth of the sector. (a) corresponds to azimuthal anisotropy strength of 20 %, while (b) corresponds to 10 %.

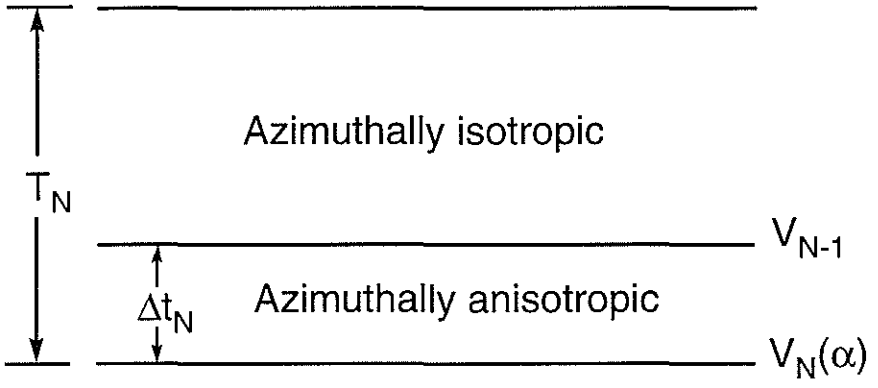

Figure 7: Schematic time section showing a model that contains an azimuthally isotropic overburden over an azimuthally anisotropic layer. Δt_N is the two-way vertical traveltime in the azimuthally anisotropic layer. The total two-way traveltime to the bottom of the azimuthally anisotropic layer is T_N, while the NMO (stacking) velocity at the top and bottom of the azimuthally anisotropic layer is denoted as V_{N-1} and V_N, respectively. The ratio $\Delta t_N/T_N = \rho$.

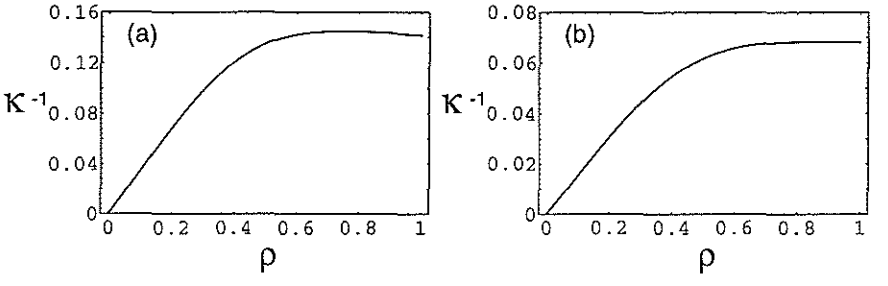

Figure 8: Plot of κ^{-1} as a function of the relative thickness ρ. $V_{N-1} = 2.0$ km/s. (a) correspond to 20% anisotropy in the azimuthally anisotropic layer where V_{s1} and V_{s2} equal to 2.4 km/s and 3.0 km/s, respectively; (b) correspond to 10% anisotropy where V_{s1} and V_{s2} equal to 2.7 km/s and 3.0 km/s, respectively. The azimuths are $\alpha_1 = 0°, \alpha_2 = 60°$, and $\alpha_3 = 120°$.

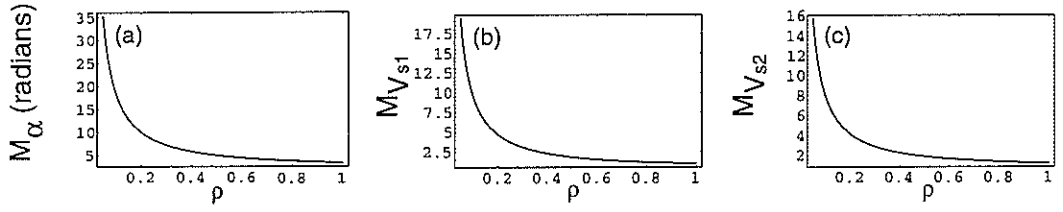

Figure 9: Magnification factors in (a) the absolute error in α measured in radians, (b) the relative error in V_{s1}, and (c) the relative error in V_{s2} as functions of the layer-thickness ratio, ρ. The selected azimuths are: $\alpha_1 = 0°$, $\alpha_2 = 60°$, and $\alpha_3 = 120°$. The model parameters are $V_{N-1} = 2.0$ km/s, and 20% anisotropy in the azimuthally anisotropic layer with V_{s1} and V_{s2} equal to 2.4 km/s and 3.0 km/s, respectively.

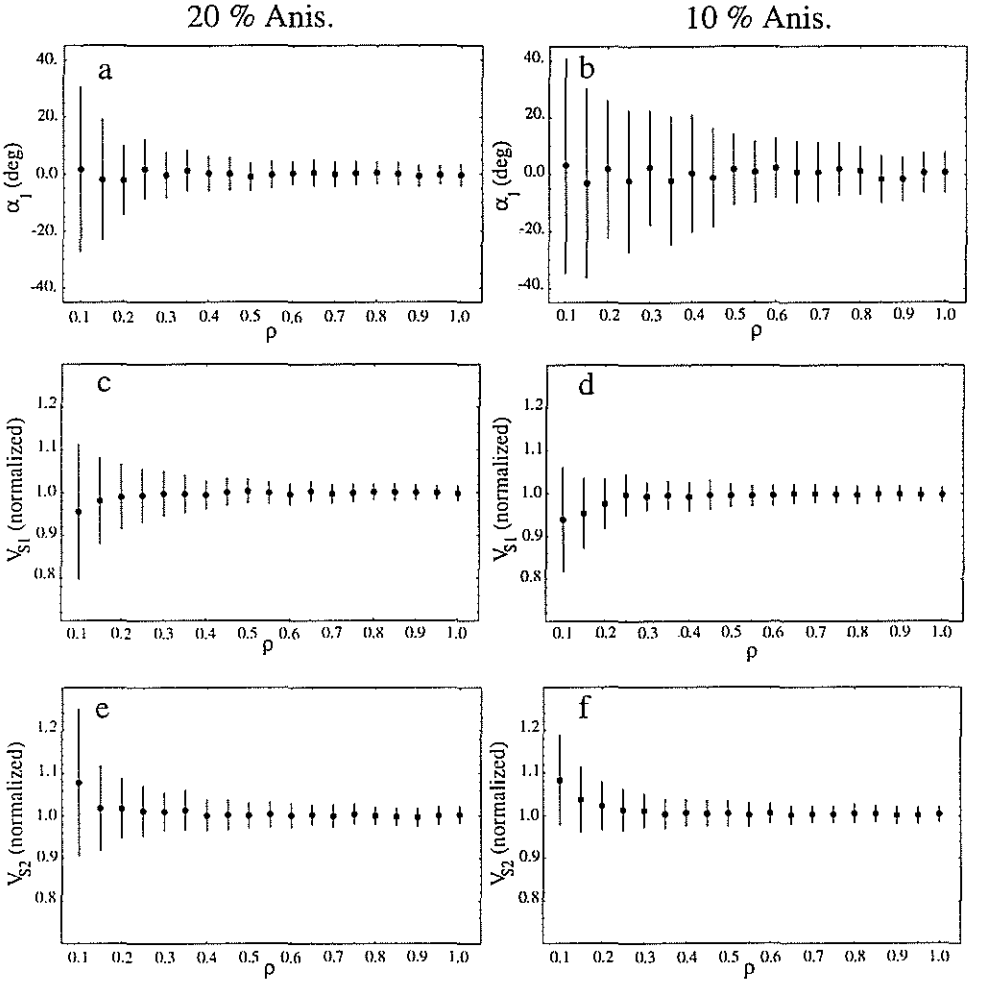

Figure 10: Estimated values for the orientation of the NMO ellipse (α_1), and for the semi-axes of the NMO ellipse (V_{s1} and V_{s2}), as well as the associated error bars as functions of the relative thickness ρ. The plots in the left column correspond to anisotropy strength of 20% ($V_{s1} = 2.4$ km/s and $V_{s2} = 3.0$ km/s), while those in the right correspond to 10% ($V_{s1} = 2.7$ km/s and $V_{s2} = 3.0$ km/s); $V_{N-1} = 2.0$ km/s. The azimuths are $\alpha_1 = 0°, \alpha_2 = 60°$, and $\alpha_3 = 120°$, measured relative to the minor semi-axis of the NMO ellipse (V_{s1}). The black dots and error bars represent the computed mean and standard deviation, respectively. The solutions for V_{s1} and V_{s2} are normalized by their true velocities.

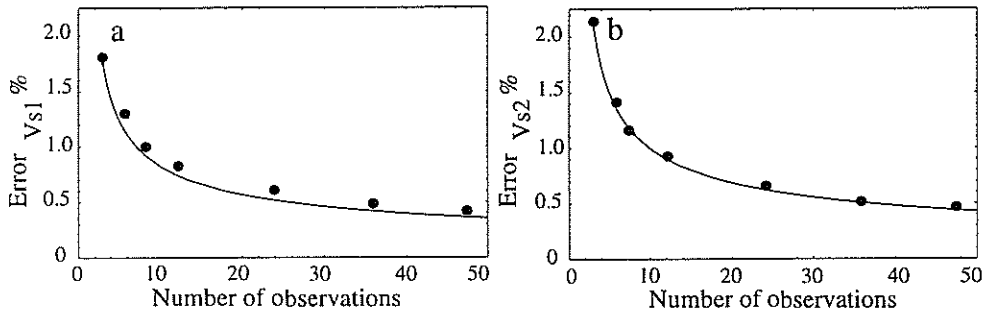

Figure 11: Estimated error, in percent, for the semi-axes of the NMO ellipse: V_{s1} (a) and V_{s2} (b) for a homogeneous azimuthally anisotropic layer, as functions of the number of observations (NMO-velocity measurements). The black dots are the least square solutions for the error bars, while the solid curve is the expected behavior with a reduction factor proportional to $1/\sqrt{(N-1)}$. Here, the strength of anisotropy is 20% ($V_{s1} = 2.4$ km/s and $V_{s2} = 3.0$ km/s).

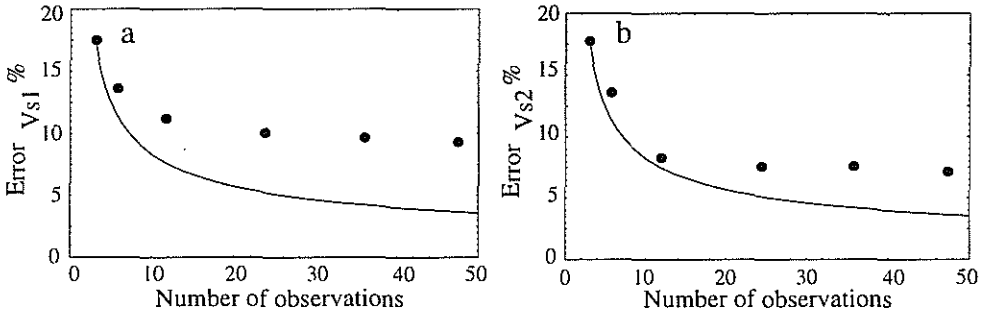

Figure 12: Estimated error, in percent, for the semi-axes of the NMO ellipse: V_{s1} (a) and V_{s2} (b) for an azimuthally anisotropic layer overlain by an azimuthally isotropic overburden, as functions of the number of observations (NMO-velocity measurements). The black dots are the least square solutions for the error bars, while the solid curve is the behavior with a reduction factor proportional to $1/\sqrt{(N-1)}$. Here, the strength of anisotropy is 20% ($V_{s1} = 2.4$ km/s and $V_{s2} = 3.0$ km/s) and the relative thickness, ρ, is 0.1. The NMO velocity at the top of the target layer is 2.0 km/s.